Quarterly Journal of the Royal Meteorological Society *Q. J. R. Meteorol. Soc.* **00: 1–11 (2018)**

Fluctuations and growth histories of cloud droplets: superparticle simulations of the collision-coalescence process†

Xiang-Yu Li*[1,2,3,4], Bernhard Mehlig[5], Gunilla Svensson[1,3], Axel Brandenburg[2,4,6], Nils E. L. Haugen[7,8]

[1]*Department of Meteorology and Bolin Centre for Climate Research, Stockholm University, Stockholm, Sweden;*
[2]*Nordita, KTH Royal Institute of Technology and Stockholm University, 10691 Stockholm, Sweden;*
[3]*Swedish e-Science Research Centre, www.e-science.se, Stockholm, Sweden;*
[4]*JILA and Laboratory for Atmospheric and Space Physics, University of Colorado, Boulder, CO 80303, USA;*
[5]*Department of Physics, Gothenburg University, 41296 Gothenburg, Sweden;*
[6]*Department of Astronomy, Stockholm University, SE-10691 Stockholm, Sweden;*
[7]*SINTEF Energy Research, 7465 Trondheim, Norway;*
[8]*Department of Energy and Process Engineering, NTNU, 7491 Trondheim, Norway;*

*Correspondence to: Xiang-Yu Li, Department of Meteorology and Bolin Centre for Climate Research, Stockholm University, Stockholm, Sweden. Email:xiang-yu.li@misu.su.se, Revision: 1.159

Direct numerical simulations of collisional aggregation in turbulent aerosols are computationally demanding. Many authors therefore use an approximate model of the collision-coalescence process that is computationally more efficient: it relies on representing physical particles in terms of 'superparticles'. One monitors collisions between superparticles and accounts for collisions between physical particles using a Monte-Carlo algorithm. It has been shown that this algorithm can faithfully represent mean particle growth in turbulent aerosols. Here we investigate how fluctuations are represented in this algorithm. We study particles of different sizes settling under gravity, assuming that the effect of turbulence is simply to mix the particles horizontally. We compute the statistics of growth histories and analyze their fluctuations in terms of the 'lucky-droplet' model. We discuss under which circumstances artefacts change the fluctuations of the growth histories, how these can be avoided, and which questions remain to be answered when turbulent fluctuations are explicitly incorporated.

Received . . .

1. Introduction

Collisions of particles in turbulent fluids play an important role in warm rain formation and planet formation. Rapid warm rain formation is still a puzzle. It is well understood that condensation dominates the growth of cloud droplets in the size range of about 2 to $15\,\mu\mathrm{m}$ (radius) without turbulence. Much larger droplets ($50\,\mu\mathrm{m}$) can grow due to collisions with small droplets as the large droplets fall through the turbulence. The question is which mechanisms cause the rapid growth of intermediate droplets, and how a sufficiently broad size distribution develops that allows for rapid runaway growth of larger (rain) droplets (Shaw 2003; Bodenschatz *et al.* 2010; Devenish *et al.* 2012; Grabowski and Wang 2013).

In the astrophysical context, an important question is how to understand the growth of dust grains to meter-sized objects and further to planetesimals, in the turbulent gas disk around a growing star (Blum and Wurm 2008; Wilkinson *et al.* 2008; Armitage 2011; Johansen and Lambrechts 2017).

The collision-coalescence process in turbulence is strongly nonlinear. Therefore, direct numerical simulations (DNS) have become an essential tool. The most natural and physical way to investigate the collisional growth is to track individual droplets and to detect their collisions. However, DNS of the collision-coalescence process are very challenging, because they must solve for the turbulence over a correspondingly large range of time and length scales. Furthermore, a numerous number ($\sim 10^8$) of individual droplets need to be tracked in both spatial and phase spaces to determine the collisions.

An alternative way of modeling the turbulent collision-coalescence process is to combine physical particles into 'superparticles' (Zsom and Dullemond 2008). To gain efficiency, one monitors only superparticle collisions and uses a Monte-Carlo algorithm (Bird 1978, 1981; Jorgensen *et al.* 1983) to account for collisions between physical particles. The superparticle approach is now widely used

in both the astrophysical literature (Zsom and Dullemond 2008; Ormel *et al.* 2009; Zsom *et al.* 2010; Johansen *et al.* 2012; Ros and Johansen 2013; Drakowska *et al.* 2014; Johansen *et al.* 2015), as well as in the meteorological literature (Andrejczuk *et al.* 2008; Shima *et al.* 2009; Andrejczuk *et al.* 2010; Patterson and Wagner 2012; Riechelmann *et al.* 2012; Arabas and ichiro Shima 2013; Naumann and Seifert 2015, 2016; Unterstrasser *et al.* 2017; Dziekan and Pawlowska 2017; Li *et al.* 2017, 2018b; Brdar and Seifert 2018).

Compared with DNS, the superparticle approach is distinctly more efficient, and it has been shown to be adequate in modeling average properties of turbulent aerosols, such as the mean collision rate: Li *et al.* (2018b) found that the mean collision rate simulated with the superparticle approach agrees well with the Saffman-Turner collision rate (Saffman and Turner 1956). Also, several studies (Shima *et al.* 2009; Unterstrasser *et al.* 2017; Li *et al.* 2017) investigated the reliability of the superparticle approach by comparing the droplet-size distribution simulated with the superparticle approach and with the Smoluchowski equation, a mean-field approach. They found good agreement.

Here we pose the question: how well do superparticle approaches account for fluctuations both in the collision sequence and the resulting aggregation process? This question is particularly important in dilute systems, such as warm rain formation and planet formation. In these systems, rare extreme events are responsible for the broadening of the size distribution. In warm rain formation, for example, the mean number density of cloud droplets is only about $n_0 = 10^8\,\mathrm{m}^{-3}$. The Kolmogorov length in cloud-like turbulence is of the order of $\eta = 1\,\mathrm{mm}$ when the mean energy dissipation rate is $\bar{\epsilon} \approx 10^{-3}\,\mathrm{m}^2\mathrm{s}^{-3}$ (Siebert *et al.* 2006). In such dilute systems, the sequence of collisions (collision time intervals) is essentially a random process with wide distributions. For example, the distribution of growth times develops extended tails as a consequence of Poisson fluctuations in the time intervals to the next collision (Telford 1955; Kostinski and Shaw 2005; Wilkinson 2016), and the distribution of turbulence-induced relative droplet velocities has power-law tails (Gustavsson and Mehlig 2011a; Gustavsson *et al.* 2014), as a consequence of caustics in the inertial-droplet dynamics (see Gustavsson and Mehlig 2016, for a review)).

To analyze how fluctuations in the collisional growth of droplets are represented in superparticle approaches, we record growth histories of individual droplets in our superparticle simulations. We store when in the past any given droplet collided and coalesced (we assume a coalescence efficiency of unity), and by how much it grew upon each collision. The ensemble of growth histories can be analyzed in different ways. It determines, for example, a distribution $P(\mathscr{T})$ of growth times $\mathscr{T}$ to a certain droplet radius r. It also yields the droplet-size distribution $f(r)$ after a certain time.

Little is known about the ensemble of growth histories–not even for limiting cases. Therefore, we restrict our analysis to a simple case: we consider droplets of different sizes settling under gravity. We assume that the effect of turbulence is simply to mix the droplets in the horizontal plane, by an average collision rate. The dynamics nevertheless exhibits substantial fluctuations, caused by the Poisson sequence of collision times between droplets of different sizes that settle at different speeds (Kostinski and Shaw 2005; Wilkinson 2016).

We do not simulate turbulent fluctuations directly, except for the simulations described at the end of this article, where we discuss some results that combine explicit modeling of turbulent fluctuations and differential settling due to gravity. The main goal of the last section is to illustrate open questions regarding the use of the superparticle approach for simulating the collision-coalescence process in turbulent aerosols.

The remainder of this paper is organized as follows. In Sec. 2 we describe the superparticle approach that is used in the present article. Sec. 3 summarizes our results for growth histories obtained using superparticle simulations of the system described above: droplets settling under gravity that are horizontally well mixed. Sec. 4 investigates the statistics of the cumulative collision time. Sec. 5 discusses the comparison of the superparticle algorithm and the mean-field Smoluchowski equation when turbulence is explicitly simulated. We conclude in Sec. 6.

2. Superparticle algorithm

Superparticle algorithms represent physical particles or droplets in terms of superparticles. All droplets in superparticle i are assumed to have the same material density ρ_d, the same radius r_i, the same velocity $\boldsymbol{v}_i$, and reside in a volume at the same position $\boldsymbol{x}_i$. The index i labels the superparticles, and it ranges from 1 to N_s (Table 1). The superparticle dynamics is explicitly modeled, taking into account gravitational and turbulent accelerations, often by simply using Stokes law. When two superparticles collide, a Monte-Carlo algorithm is used to describe collisions between the droplets contained in the superparticles. Different collision schemes have been suggested in the literature for this purpose, starting with Zsom and Dullemond (2008), Andrejczuk *et al.* (2008), and Shima *et al.* (2009). Table 2 lists those that have been used most frequently. This table distinguishes between symmetric and asymmetric schemes, depending on whether or not the algorithm is invariant under the exchange of superparticles.

Unterstrasser *et al.* (2017) compared three different collision schemes used mainly in the meteorology community. They compared the droplet-size distribution simulated from the superparticle algorithm and the mean-field Smoluchowski equation. They found that only the scheme of Shima *et al.* (2009) can correctly represent the mean droplet growth. Zsom and Dullemond (2008) may have been the first to develop a superparticle algorithm to tackle collisions of particles, even though momentum is not conserved in their algorithm (A. Johansen, 2016, private communication). Li *et al.* (2017) described differences between the symmetric superparticle algorithm developed by Shima *et al.* (2009) and the asymmetric one developed by Johansen *et al.* (2012). It turns out that the scheme used by Shima *et al.* (2009) results in slightly better statistics. Here we therefore employ this scheme.

Table 1. Definition of variables in superparticle algorithm.

N_s	Number of 'superparticles'
$N_\mathrm{d/s}$	Number of droplets in a superparticle
$N_\mathrm{tot} = N_\mathrm{d/s} N_\mathrm{s}$	Total number of droplets

Table 2. Summary of different superparticle algorithms.

Reference	mass conservation	momentum conservation	collision symmetry	stochasticity
Zsom and Dullemond (2008)	yes	no	asymmetric	probabilistic
Shima *et al.* (2009)	yes	yes	symmetric	probabilistic
Andrejczuk *et al.* (2008)	yes	yes	asymmetric	deterministic
Riechelmann *et al.* (2012)	yes	yes	asymmetric	deterministic
Johansen *et al.* (2012)	yes	yes	asymmetric	probabilistic

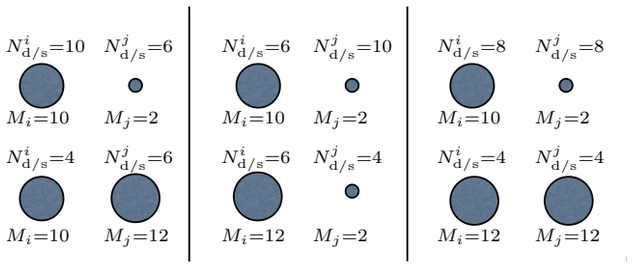

Figure 1. Collision outcomes when two superdroplets collide and particle collisions occur. Superparticle i contains $N^i_{\rm d/s}$ droplets of mass M_i, superparticle j contains $N^j_{\rm d/s}$ droplets of mass M_j. After the collision, the superdroplet with the larger droplets inherits the identity of the superdroplet that had larger particles before the collision. This is not shown.

Our simulations are conducted using the PENCIL CODE. The equation of motion for the position $\boldsymbol{x}_i$ and velocity $\boldsymbol{v}_i$ of superparticle i reads:

$$\frac{{\rm d}\boldsymbol{x}_i}{{\rm d}t} = \boldsymbol{v}_i\,, \quad \frac{{\rm d}\boldsymbol{v}_i}{{\rm d}t} = \frac{1}{\tau_i}(\boldsymbol{u}-\boldsymbol{v}_i) + \boldsymbol{g}\,. \tag{1}$$

Here $\boldsymbol{g}$ is the gravitational acceleration. Further,

$$\tau_i = 2\rho_{\rm d} r_i^2/[9\rho\nu\, C(Re_i)] \tag{2}$$

is the particle response time attributed to the superparticle, and ρ is the mass density airflow. The correction factor $C(Re_i) = 1 + 0.15\,{\rm Re}_i^{2/3}$ models the effect of non-zero particle Reynolds number ${\rm Re}_i = 2r_i|\boldsymbol{u}-\boldsymbol{v}_i|/\nu$ (Schiller and Naumann 1933; Marchioli *et al.* 2008). Finally, $\boldsymbol{u}$ is the turbulent velocity at the particle position. In sections III and IV, turbulence is not explicitly modeled, in these sections $\boldsymbol{u} = 0$.

Droplet collisions are represented by collisions of superparticles (Johansen *et al.* 2012), as explained above. When two superparticles collide, a Monte-Carlo scheme is used to determine which pairs of droplets collide. It is assumed that two droplets in either of the superparticles (with indices i and j) collide with probability

$$p_{ij} = \lambda_{ij}\Delta t\,, \tag{3}$$

where Δt is the integration time step. In the model of Shima *et al.* (2009), the collision rate is

$$\lambda_{ij} = E_{ij}\pi\left(r_i + r_j\right)^2 |\boldsymbol{v}_i - \boldsymbol{v}_j|\, N_{\rm d/s}\, \delta x^{-3}\,, \tag{4}$$

where $N_{\rm d/s}$ is the larger initial number of droplets per superparticle i or j (Table 1), and δx^3 is the volume assigned to the superparticle. Moreover, E_{ij} is the collision efficiency assumed to be unity in this article.

What happens when two superparticles collide? To write down the rules, we denote the number of droplets in superparticle i by $N^i_{\rm d/s}$, while $N^j_{\rm d/s}$ is the number of droplets in superparticle j. M_i and M_j are the corresponding droplet masses. The collision scheme suggested by Shima *et al.* (2009) amounts to the following rule. To ensure mass conservation between superparticles i and j, when $N^j_{\rm d/s} > N^i_{\rm d/s}$, droplet numbers and masses are updated as

$$\begin{aligned} N^i_{\rm d/s} &\to N^i_{\rm d/s}\,, \quad N^j_{\rm d/s} \to N^j_{\rm d/s} - N^i_{\rm d/s}\,, \\ M_i &\to M_i + M_j\,, \quad M_j \to M_j\,. \end{aligned} \tag{5}$$

When $N^j_{\rm d/s} < N^i_{\rm d/s}$, the update rule is also given by equation (5), but with indices i and j exchanged. In other words, the number of particles in the smaller superparticle remains unchanged (and their masses are increased), while that in the larger one is reduced by the amount of particles that have collided with all the particles of the smaller superparticle (and their masses remain unchanged). This is illustrated in Figure 1. Finally, when $N^j_{\rm d/s} = N^j_{\rm d/s}$, droplet numbers and masses are updated as

$$\begin{aligned} N^i_{\rm d/s} &\to N^i_{\rm d/s}/2\,, \quad N^j_{\rm d/s} \to N^j_{\rm d/s}/2\,, \\ M_i &\to M_i + M_j\,, \quad M_j \to M_i + M_j\,. \end{aligned} \tag{6}$$

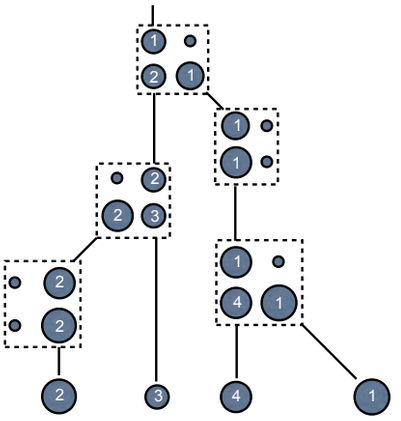

Figure 2. Superparticle identities and coalescent process of collision histories. All collisions involve one 10μm-droplet. Collisions (between pairs of particles) are illustrated by a dashed box. Superparticles that contain large droplets are shown with larger radii. The histories of superparticles 2, 3 and, 4 cannot be tracked all the way back.

To ensure momentum conservation during the collision, the momenta of particles in the two superparticles are updated as

$$\begin{aligned} \boldsymbol{v}_i M_i &\to \boldsymbol{v}_i M_i + \boldsymbol{v}_j M_j \,, \\ \boldsymbol{v}_j M_j &\to \boldsymbol{v}_j M_j \,, \end{aligned} \tag{7}$$

after a collision of superparticles.

The collision scheme described here is symmetric in the sense that collisions take place simultaneously in both superparticles i and j, so that $p_{ij} = p_{ji}$ and, correspondingly, $\lambda_{ij} = \lambda_{ji}$. This is due to the fact that λ_{ij} described in equation (4) is always determined by the largest $N_{\mathrm{d/s}}$ as discussed right below equation (4). By contrast, in Johansen *et al.* (2012), collisions only occur in superparticle j, which is referred to as asymmetric collision (Li *et al.* 2017). In addition, collisions are probabilistic, as described by equation (3). On the other hand, the collision schemes of the superparticle approach developed in Andrejczuk *et al.* (2008) and Riechelmann *et al.* (2012) are deterministic. We refer to Table 2 for a detailed comparison of different superparticle approaches.

In the example discussed in section 1, there is only one droplet in a 10η-sized volume, so that the probability that this droplet can collide with another one is very low unless there is horizontal mixing of droplets. We can assume that the rate λ represents this horizontal mixing due to the mean effect of turbulence. For small droplets, it is described by the Saffman-Turner rate (Saffman and Turner 1956; Brunk *et al.* 1998; Andersson *et al.* 2007) due to turbulent shear. For larger droplets, the effect of particle inertia must be considered (Wilkinson *et al.* 2006; Gustavsson and Mehlig 2011b; Gustavsson *et al.* 2015; Gustavsson and Mehlig 2016).

We emphasize that the superparticle algorithm is stochastic if p_{ij} is small enough, so that most superparticle collisions do not lead to particle collisions.

3. Growth histories

We consider one $12.6\,\mu$m-droplet within a cloud of $10\,\mu$m-droplets. Since the larger droplet is somewhat heavier, it falls more rapidly than the $10\,\mu$m-droplets and sweeps them up through collisions and coalescences. Collisions are driven by differential settling, therefore $10\,\mu$m-droplets cannot collide with each other. Here, turbulence is not explicitly modeled, i.e., $\boldsymbol{u} = 0$ in equation (1). We repeat the simulation many times using different sequences of random numbers, to obtain an ensemble of growth histories of $12.6\,\mu$m droplets.

The collision histories are tracked in the following way. We record and output the collision histories for all superparticles during the simulation. Of particular interest is the fastest growing droplet. We trace its growth history backwards in time by finding its parents for each collision that occurred during its growth history in the past. This is illustrated in Figure 2. Collisions (between pairs of particles) are illustrated by a dashed box. Superparticles that contain large droplets are drawn with larger radii. Each superparticle is initially assigned an identification number (ID). Superparticle IDs are given by white numbers. Since we are interested in the fastest growing droplet, it is convenient to require that the larger superparticle after the collision inherits the ID of the larger superparticle before the collision. In some cases (three out of five in Figure 2) this means that the IDs are exchanged during a collision.

Figure 3 shows an ensemble of growth histories (thin grey lines) obtained from independent simulations as described above. The times between collisions are random, leading to a distribution of cumulative growth times to reach $50\,\mu$m. Also shown is the mean growth curve (thick black line), obtained by averaging the time at fixed radii r. The Figure demonstrates that the fluctuations are substantial.

Figure 4 shows one particular growth history from Figure 3. It is expected that the growth steps (in r) become smaller and smaller as time proceeds, because the numerical experiment was designed such that all collisions occur with $10\,\mu$m-droplets. However, Figure 4 shows that larger jumps occur later in the growth history. These jumps are artefacts caused by the collision scheme described in Sec. 2, as we discuss now.

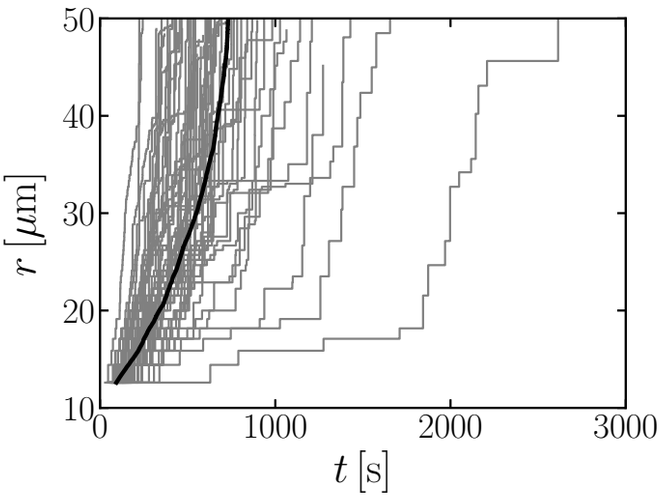

Figure 3. Shows an ensemble of 50 growth histories obtained from independent simulations as described in the text. Initial condition: all superparticles have the same number of droplets, $N_{\mathrm{d/s}} = 2$.

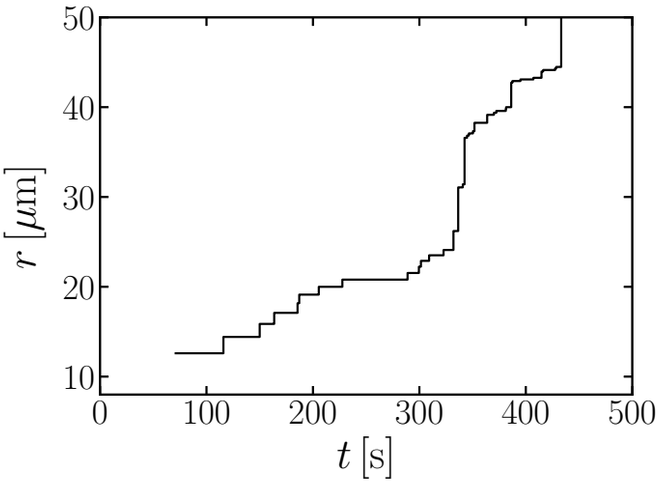

Figure 4. Shows a growth history taken from from Figure 3.

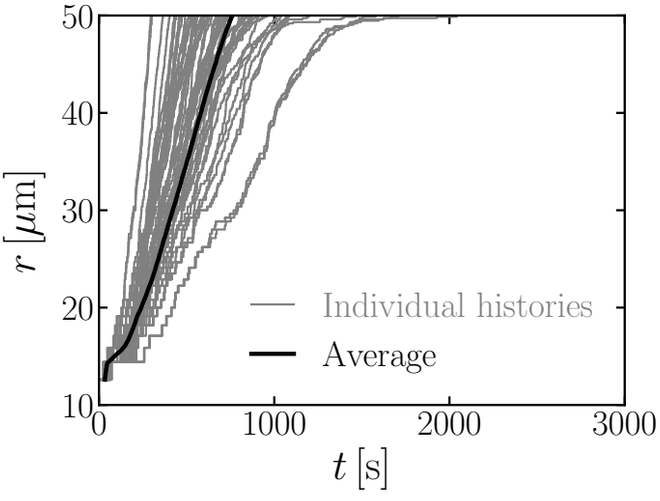

Figure 5. Shows an ensemble of 50 growth histories similar to Figure 3, but for a different initial condition. For the $12.6\,\mu$m-sized superparticle we take $N_{\mathrm{d/s}} = 2$, and for $10\,\mu$m-sized superparticles, $N_{\mathrm{d/s}} = 40$.

Figure 1 shows examples of collision outcomes when a superparticle containing larger droplets collides with a superparticle containing $10\,\mu$m-sized droplets. In two cases (leftmost and rightmost in Figure 1) the droplets in both superparticles grow, a

consequence of the scheme summarized in equations (5) and (6). The growth of the smaller $10\,\mu\mathrm{m}$ droplets is artificial, because the numerical experiment was designed so that this cannot occur. These artefacts give rise to superparticles with larger droplets. Later collisions cause larger jumps in the growth history, as shown in Figure 1. Figure 2 illustrates another aspect of these artefacts: they occur precisely when the superparticle IDs are exchanged upon collision.

One way of avoiding these artefacts, or at least of ensuring that they occur rarely, is to use initial conditions that mostly yield collisions corresponding to the case shown in the center of Figure 1. This can be achieved by choosing the number $N_{\mathrm{d/s}}$ of droplets in the $10\,\mu\mathrm{m}$ superparticle to be much larger than that in the $12.6\,\mu\mathrm{m}$ superparticle. Artefacts will first occur at later times when these numbers become equal. As the simulation proceeds, the number of droplets per superparticle decreases for the $10\,\mu\mathrm{m}$-sized superparticle. When $N_{\mathrm{d/s}}$ becomes equal for the large superparticle and a $10\,\mu\mathrm{m}$-sized superparticle, both superparticles grow as the middle panel of Figure 1 shows. Therefore, the frequency of artefacts increases with time.

In Figure 3, by contrast, all superparticles contain the same number of droplets initially, as described in the caption of Figure 5, which shows the corresponding simulations for different initial conditions, where $N_{\mathrm{d/s}} = 2$ for the $12.6\,\mu\mathrm{m}$-sized superparticle, and $N_{\mathrm{d/s}} = 40$ for the $10\,\mu\mathrm{m}$-sized superparticle. No artefacts have occurred–at least up to $r = 50\,\mu\mathrm{m}$. Since $N_{\mathrm{d/s}} = 2$ for $10\,\mu\mathrm{m}$-sized superparticles in Figure 3, while $N_{\mathrm{d/s}} = 40$ in Figure 5, the collision rate for the latter case is 20 times large than the former case according to equations (3) and (4). Therefore, we scale the time in Figure 5 by a factor of 20. Let us compare the ensemble of growth histories shown in Figures 3 and 5. We see that the histories in Figure 5 do not exhibit artificial jumps. Therefore the fastest growing droplets in Figure 5 grow slower than those in Figure 3. But we also see that the ensemble in Figure 3 contains several histories corresponding to droplets that grow very slowly. These are absent in Figure 5. This may be an artefact due to the large initial number density used in Figure 5. Thus, there is a trade-off between the two different types of artifacts occurring in Figure 3 and Figure 5.

We checked that the asymmetric collision scheme proposed by Johansen *et al.* (2012) also reveals artificial jumps due to the mass conservation scheme.

4. Statistics of cumulative collision times

We now determine the statistics of the cumulative collision time $\mathscr{T}$, for one larger droplet with radius $12.6\,\mu\mathrm{m}$ falling through the ensemble of $10\,\mu\mathrm{m}$-sized droplets, as described above. We trace the collision history of the $12.6\,\mu\mathrm{m}$ droplet and compute the cumulative time until the $\mathscr{N}$-th collision occurs:

$$\mathscr{T}_{\mathscr{N}} = \sum_{k=1}^{\mathscr{N}} t_k \,. \tag{8}$$

The times t_k between successive collisions are exponentially distributed, with rates λ_k:

$$p_k(t_k) = \lambda_k \exp(-\lambda_k t_k). \tag{9}$$

The larger droplet grows by collisions with $10\,\mu\mathrm{m}$ droplets. At the k-th collision, the initial droplet volumes have increased by a factor of k, and the radius increased by a factor of $k^{1/3}$, so $r_k \sim r_0 k^{1/3}$. The rates λ_k depend on the differential settling velocity $(\boldsymbol{v}_i - \boldsymbol{v}_j)$ between the colliding droplets through equations (3) and (4). Considering a droplet sediment in a stagnant flow, the amplitude of the terminal velocity is $|\boldsymbol{v}_i| = \tau_i g$ according to equation (1). In this case, the correction factor $C(Re_i)$ is approximated to one in equation (2). Therefore, $|\boldsymbol{v}_i| \sim r_i^2$. Since we assumed that the collision efficiency E_{ij} is unity, equation (4) can be approximated as $\lambda_{ij} \sim r_j^4$ assuming $r_j \gg r_i$. In terms of the number of collision k, it follows that

$$\lambda_k = \lambda_1 k^{4/3} \,. \tag{10}$$

This is precisely the 'lucky-droplet' model suggested by Kostinski and Shaw (2005) and further developed by Wilkinson (2016), designed to describe the situation we consider in the numerical experiments described above.

We now determine whether the superparticle algorithm correctly represents the distribution $P(\mathscr{T})$. We note that $\langle\mathscr{T}\rangle$ is determined by λ_1, which describes the horizontal mixing of droplets by the mean turbulent shear, in the absence of turbulent fluctuations. Since $\tau = \mathscr{T}/\langle\mathscr{T}\rangle$ is independent of λ_1, we mainly focus on determining $P(\tau)$ in the following.

To compute the distribution of cumulative collision times $\mathscr{T}$, we performed 1059 simulations with different random seeds. For each simulation, we tracked the growth history of the droplet that first reached $50\,\mu\mathrm{m}$ and recorded the time $\mathscr{T}_{50}$ it took to grow to $50\,\mu\mathrm{m}$. Figure 6 shows $P(\tau)$. We checked that no artefacts occurred during the simulations. The Figure shows that the results of the superparticle simulations agree fairly well with equations (8) and (10). To obtain the corresponding result, we simulated 10^8 realizations of these equations.

In summary, stochastic fluctuations in the superparticle algorithm are caused by the Monte-Carlo collision scheme. The Monte-Carlo scheme is parameterized by the rate λ_{ij} in equation (4). This rate can be interpreted as a collision rate representing the horizontal mixing of settling droplets in a mean-field fashion. In this way the superparticle scheme can accurately represent the growth histories of the lucky-droplet model (Kostinski and Shaw 2005). Poisson fluctuations of the times between collisions give rise to a distribution of cumulative collision times in the lucky-droplet model. In the numerical experiments described above, the growth histories fluctuate in the same way as described in the lucky-droplet models mentioned above.

We have also calculated $P(\tau)$ for initial conditions where artefacts occur as shown by the black curve in Figure 6. The corresponding jumps in the growth histories cause the droplets to grow faster. However, it turns out that the artefacts do not have noticeable effect upon $P(\tau)$ in the simulations we conducted. This could be because there were simply too few artefacts to make a noticeable difference. A more likely explanation is that the artefacts occur quite late in the growth history. Kostinski and Shaw (2005) explained that fluctuations in the collisional growth of settling droplets are largely determined by the first few collisions. Therefore late jumps do not matter so much.

We mention that Dziekan and Pawlowska (2017) investigated related questions. They studied the stochastic coalescence of settling droplets, comparing the superparticle algorithm with the mean-field Smoluchowski equation. They found good agreement between

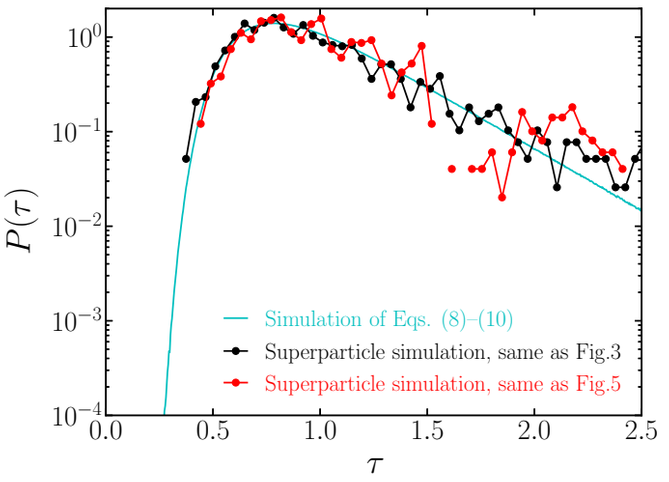

Figure 6. Distribution of τ. The red curve represents $P(\tau)$ obtained from 1059 superparticle simulations (same simulations as in Figure 5) The cyan curve represents the simulation of equation (9), equation (8), and equation (10) with $\lambda_1 = 1\,\mathrm{s}^{-1}$ and $\mathcal{N} = 128$ (see text), where 10^8 realizations are simulated.

the superparticle algorithm and the Smoluchowski equation by comparing the droplet-mass distribution function, thus, concluding that the superparticle algorithm can represent the stochastic coalescence. However, they did not track collision histories of superparticles. Furthermore, they used an exponential initial distribution of droplet-sizes, quite different from our initial conditions. Since we saw that the initial conditions affect how frequently artefacts occur, it is important to study how accurately fluctuations are represented for a range of different initial conditions.

5. Simulations with turbulence explicitly modeled

The effect of turbulence on collisional growth of cloud droplets is still debated. The typical Stokes number is $\mathrm{St} \approx 0.02$ for $10\,\mu$m-sized droplets such that clustering (Bec *et al.* 2007; Gustavsson and Mehlig 2016) and caustics (Falkovich *et al.* 2002; Wilkinson *et al.* 2006; Gustavsson *et al.* 2012) are too weak to play a role for such small droplets (Gustavsson and Mehlig 2014; Voßkuhle *et al.* 2014).

To illustrate how turbulence may impact the random growth process, we conducted simulations in the same manner as described above, but with turbulence fluctuations added. In the absence of turbulence fluctuations, the $12.6\,\mu$m-droplet only collides with $10\,\mu$m-sized droplets. When turbulence fluctuations are present, the $12.6\,\mu$m-droplet may also collide with droplets larger than $10\,\mu$m, which results in faster growth.

It is worth noting that the fastest growing droplet need not to be the one with initial radius $r = 12.6\,\mu$m when turbulence is present. This is because vigorous eddies may generate the first few droplets that end up growing most rapidly (Kostinski and Shaw 2005).

Perhaps the best way to examine how turbulence influences the lucky droplet model is to repeat the simulations with different random seeds. However, with turbulence being sufficiently well resolved, this is not feasible computationally using the modern supercomputer. A second problem is that we do not know how to reliably get rid of the aforementioned artefacts when turbulence is explicitly modeled. This is important, because larger jumps that occur early on in the growth history can substantially affect the fluctuations of the cumulative collision time $\mathscr{T}$. Later jumps may not matter as much (Kostinski and Shaw 2005), neither those due to artefacts nor those due to turbulence. A third problem is the interpretation of λ_{ij}. In the numerical experiments described in the previous sections, we could interpret these rates as the horizontal turbulent mixing rates. When turbulence is represented explicitly, it is not clear that this interpretation remains appropriate.

Despite these open questions we performed superparticle simulations, explicitly modeling turbulent fluctuations. Details are given in (Li *et al.* 2017); see also Appendix A for the essentials. We compared the droplet-size distribution from the superparticle simulation with a mean-field approach, the Smoluchowski equation described in Appendix B. It is worth mentioning that simulations of the Smoluchowski equation is computationally demanding, because a separate momentum equation has to be solved for each particle size; see details in (Li *et al.* 2017). Therefore, the simulation of the Smoluchowski equation is nearly well-resolved such that $\delta x \approx 2\eta$. Since no collisions can occur in the mean-field model without initial size differences, we adopt a log-normal initial size distribution (appendix B). The results are shown in Figure 7. We see that the tails of the size distribution obtained from the superparticle simulations with turbulent fluctuations (details in Appendix A) are wider than that obtained from the mean-field Smoluchowski equation. At present we do not know which mechanisms cause the extended tails in the superparticle simulations. They could be due to turbulent fluctuations, but could also be caused by the artefacts described above. To answer this question it is necessary to resolve the three questions posed at the beginning of this section.

6. Conclusions

We investigated growth histories of droplets settling under gravity using superparticle simulations. The goal was to determine how accurately these simulations represent the fluctuations of the growth histories. The superparticle algorithm represents droplets in terms of superparticles. Superparticle collisions are monitored, while droplet collisions are modelled by a Monte Carlo scheme, parameterized by the mean-field collision rate given by equation (4). This rate can be interpreted as a horizontal mixing rate due to turbulent shear, when turbulence is not explicitly represented. We determined the fluctuations of growth histories in this model, and showed that artefacts due to the collision scheme may give rise to faster growth and larger fluctuations. Another type of artifact occurs in dense systems,

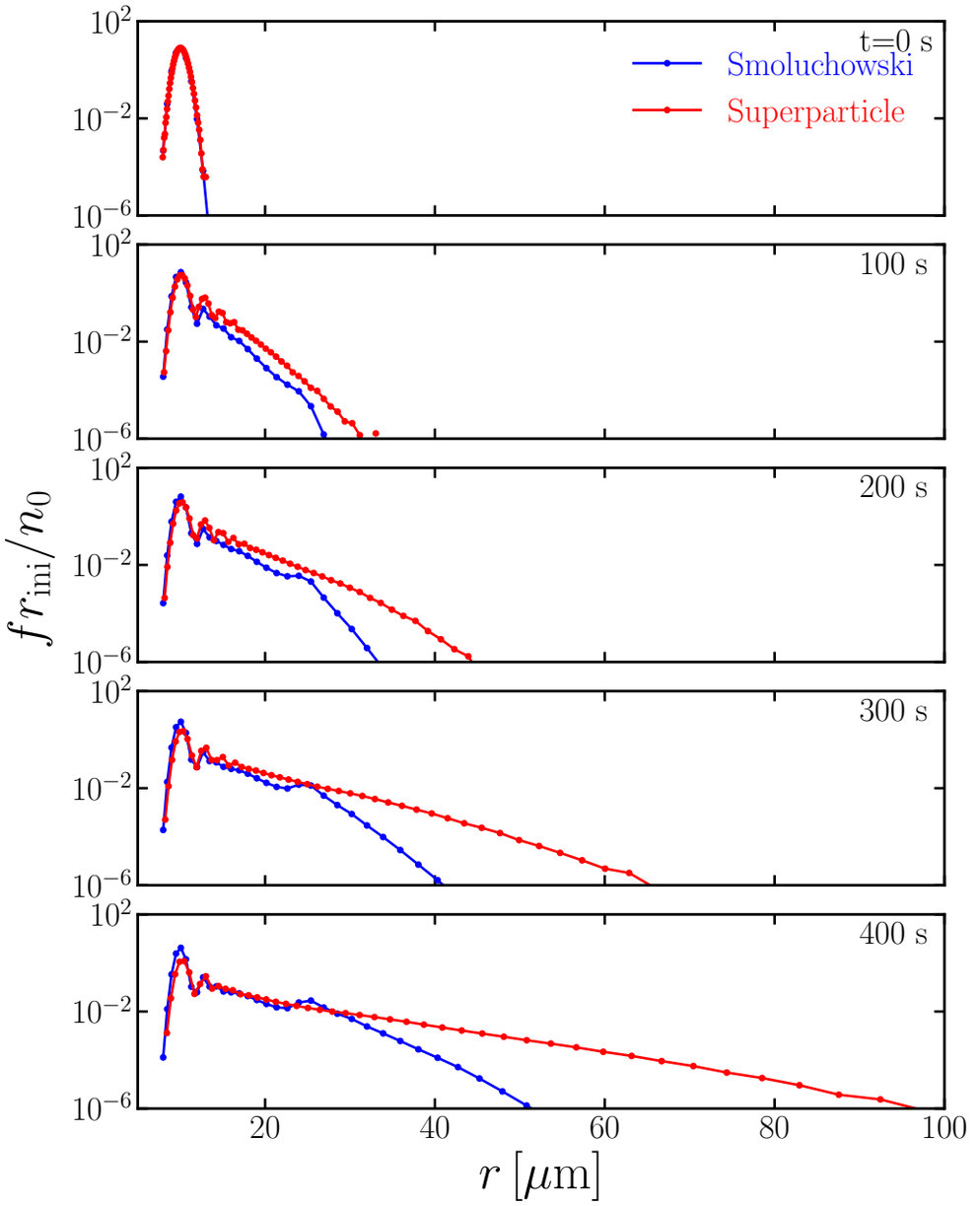

Figure 7. Comparison of the droplet-size distribution simulated from the Smoluchowski equation and the superparticle algorithm, in which turbulence fluctuations are explicitly modelled; see Runs C and D for simulation details.

which suppress fluctuations. We explained that the artefacts are a result of the collision scheme used in the superparticle algorithm, and showed that the frequency at which the artefacts occur depends on the initial conditions. For these numerical experiments, the form of the distribution $P(\mathscr{T})$ of cumulative growth times is known (Kostinski and Shaw 2005; Wilkinson 2016). In the absence of artefacts, the superparticle algorithm reproduces this form. Also, it is necessary to check whether the collision scheme by Zsom and Dullemond (2008), Andrejczuk *et al.* (2008), and Riechelmann *et al.* (2012) give rise to artefacts similar to the ones we have discussed, or not.

When turbulence is incorporated explicitly, many questions remain. First, it is unclear how to interpret the meaning of the Monte-Carlo rate λ_{ij} that parameterizes the rate at which droplet collisions occur. Second, it is necessary to investigate how the above-mentioned artefacts can be avoided when turbulence is explicitly represented. These are technical questions concerning the superparticle algorithm. The main physical question is under which circumstances do turbulent fluctuations affect the early collision histories and thus contribute significantly to the fluctuations in the aggregation process. We expect that turbulent fluctuations matter more when the turbulent aerosol is denser. But the technical questions regarding superparticle algorithms need to be resolved before we can attack this question. We intend to perform direct numerical simulations with and without the superparticle approximation, to definitely determine under which circumstances superparticle algorithms work well. This is a very important question, because direct numerical simulations are computationally very challenging. It is highly desirable to have an efficient and accurate alternative.

Acknowledgements

This work was supported through the FRINATEK grant 231444 under the Research Council of Norway, SeRC, the Swedish Research Council grants 2012-5797, 2013-03992, and 2017-03865, Formas grant 2014-585, by the University of Colorado through its support

Table 3. Summary of the simulations.

Run	model	turbulence	f_0	L (m)	$N_{\rm grid}$	$N_{\rm s}$	n_0	$N_{\rm p/s}$	$u_{\rm rms}\,({\rm m\,s^{-1}})$	${\rm Re}_\lambda$	$\bar{\epsilon}\,({\rm m^2 s^{-3}})$	$\eta\,({\rm mm})$
A	Superparticle	implicit	–	0.0096	–	128	2.97×10^8	2	–	–	–	–
B	Superparticle	implicit	–	0.0096	–	128	5.94×10^9	40	–	–	–	–
C	Superparticle	explicit	0.02	0.125	256^3	1953120	5.94×10^9	5	0.163	44	0.040	0.5
D	Smoluchowski equation	–	0.02	0.125	128^3	–	2.5×10^{10}	–	0.166	58	0.037	0.44

of the George Ellery Hale visiting faculty appointment, and by the grant "Bottlenecks for particle growth in turbulent aerosols" from the Knut and Alice Wallenberg Foundation, Dnr. KAW 2014.0048. The simulations were performed using resources provided by the Swedish National Infrastructure for Computing (SNIC) at the Royal Institute of Technology in Stockholm and Chalmers Centre for Computational Science and Engineering (C3SE). This work also benefited from computer resources made available through the Norwegian NOTUR program, under award NN9405K. The source code used for the simulations of this study, the PENCIL CODE, is freely available on `https://github.com/pencil-code/`.

A. DNS of the turbulent air flow

The purpose of this appendix is to provide more detail regarding the turbulent air flow simulation discussed in section 5. For completeness, we summarize here the basics of the simulations that we used already in our earlier work (Li *et al.* 2017, 2018b,c,a). The velocity $\boldsymbol{u}$ of the turbulent air flow is determined by the Navier-Stokes equations,

$$\frac{\partial \boldsymbol{u}}{\partial t} + \boldsymbol{u}\cdot\boldsymbol{\nabla}\boldsymbol{u} = \boldsymbol{f} - \rho^{-1}\boldsymbol{\nabla}p + \rho^{-1}\boldsymbol{\nabla}\cdot(2\nu\rho\mathsf{S}), \tag{11}$$

$$\frac{\partial \rho}{\partial t} + \boldsymbol{\nabla}\cdot(\rho\boldsymbol{u}) = 0, \tag{12}$$

where $\boldsymbol{f}$ is a monochromatic random forcing function (Brandenburg 2001) with amplitude f_0, ν is the kinematic viscosity of the air flow, $\mathsf{S}_{ij} = \frac{1}{2}(\partial_j u_i + \partial_i u_j) - \frac{1}{3}\delta_{ij}\boldsymbol{\nabla}\cdot\boldsymbol{u}$ is the traceless rate-of-strain tensor, p is the gas pressure, and ρ is the gas density. We use the Taylor microscale Reynolds number to characterize the intensity of turbulence, ${\rm Re}_\lambda \equiv u_{\rm rms}^2\sqrt{5/(3\nu\bar{\epsilon})}$, where $u_{\rm rms}$ is the rms turbulent velocity, and $\bar{\epsilon} = 2\nu\,\overline{{\rm Tr}\,\mathsf{S}_{\rm ij}^{\sf T}\mathsf{S}_{\rm ij}}$ is the mean energy-dissipation rate per unit mass and Tr denotes the trace. The superparticle simulation is well-resolved such that $\delta x \approx \eta$, where $\delta x = L/N_{\rm grid}^{1/3}$ is the side length of the grid cell of our DNS, and $N_{\rm grid}$ is the number of the grid cells. The volume of each superparticle is $(\delta x)^3$, i.e., η^3, which is the smallest physical volume in DNS that one can choose. More importantly, to solve the momentum equation of superparticles given by equation (1), one needs to map the fluid velocity to the velocity of superparticles. The parameters of all simulations are listed in Table 3.

B. Smoluchowski equation

We present here the Smoluchowski equation discussed in section 5. The Smoluchowski equation has been widely used to simulate the collisional growth of cloud droplets. It is a mean-field approach because fluctuations are neglected. Collision-coalescence is governed by the Smoluchowski equation

$$\begin{aligned}\frac{Df}{Dt} &= \tfrac{1}{2}\int_0^m K(m-m',m')\,f(m-m')\,f(m')\,{\rm d}m' \\ &- \int_0^\infty K(m,m')\,f(m)\,f(m')\,{\rm d}m',\end{aligned} \tag{13}$$

where $D/Dt = \partial/\partial t + \boldsymbol{v}\cdot\boldsymbol{\nabla}$ is the material derivative, and K is the collision kernel, which is proportional to the collision efficiency $E(m,m')$ and a geometric contribution. As mentioned above, we assume $E=1$ and so K is given by

$$K(m,m') = \pi(r+r')^2|\boldsymbol{v}-\boldsymbol{v}'|, \tag{14}$$

where r and r' are the radii of the corresponding mass variables, m and m', while $\boldsymbol{v}$ and $\boldsymbol{v}'$ are their respective velocities, whose governing equation is given below. The Smoluchowski equation is a mean-field equation in the sense that the droplet-size distribution solved in equation (13) is assumed to be spatially uniform. Also, it only involves mean collision kernels.

We define the mass and radius bins such that

$$m_k = m_1\delta^{k-1}, \quad r_k = r_1\delta^{(k-1)/3}, \tag{15}$$

where $\delta = 2^{1/\beta}$. Here β is a parameter that we chose to be a power of two. For a fixed mass bin range, the number of mass bins $k_{\rm max}$ increases with increasing β. In the simulation reported in Sec. 5, we set $k_{\rm max} = 61$ with $\beta = 4$.

The velocities of the particle fluid $\boldsymbol{v}_k$ is obtained by solving momentum equations, $\boldsymbol{v}_k(\boldsymbol{x},t) = \boldsymbol{v}(\boldsymbol{x},\ln m_k,t)$ for each logarithmic mass value $\ln m_k$ is

$$\frac{\partial \boldsymbol{v}_k}{\partial t} + \boldsymbol{v}_k\cdot\boldsymbol{\nabla}\boldsymbol{v}_k = \boldsymbol{g} - \frac{1}{\tau_k}(\boldsymbol{v}_k - \boldsymbol{u}) + \boldsymbol{F}_k(\boldsymbol{v}_k), \tag{16}$$

where $1 \le k \le k_{\rm max}$, τ_k (for $k=i$) is defined by equation (2), and

$$\boldsymbol{F}_k(\boldsymbol{v}_k) = \nu_{\rm p}\nabla^2\boldsymbol{v}_k \tag{17}$$

is a viscous force of the particle fluid, which is due to the interaction between the individual particles. Here $\nu_{\rm p} = 10^{-3}\,{\rm m}^2\,{\rm s}^{-1}$ is the artificial viscosity. This viscous force should be very small for dilute particle suspensions, but is nevertheless retained in equation (16) for the sake of numerical stability of the code.

Since collisions can only happen if droplets have different sizes when using the Smoluchowski equation, the initial condition used in the superparticle approach is not applicable. Instead, we adopt a log-normal droplet-size distribution (Nenes and Seinfeld 2003; Seinfeld and Pandis 2016) for both the Smoluchowski equation and the superparticle approach. The log-normal droplet-size distribution is widely used in climate models and is supported by the in situ atmospheric measurements (Miles *et al.* 2000),

$$f(r,0) = \frac{n_0}{\sqrt{2\pi}\sigma_{\rm ini}\, r}\, \exp\Big[- \frac{\ln^2(r/r_{\rm ini})}{2\sigma_{\rm ini}^2}\Big]\,. \tag{18}$$

Here $r_{\rm ini} = 10\,\mu$m and $\sigma_{\rm ini} = 0.05$ is the width. Since the Smoluchowski equation is extremely computationally demanding (2.8 s simulation time with 24 hours wall-clock time on 2048 CPUs), we use $n_0 = 2.5 \times 10^{10}\,{\rm m}^{-3}$ for the Smoluchowski equation.

References

Andersson B, Gustavsson K, Mehlig B, Wilkinson M. 2007. Advective collisions. *Europhys. Lett.* **80**. 69001.

Andrejczuk M, Grabowski WW, Reisner J, Gadian A. 2010. Cloud-aerosol interactions for boundary layer stratocumulus in the lagrangian cloud model. *Journal of Geophysical Research: Atmospheres* **115**(D22): n/a–n/a, doi:10.1029/2010JD014248, URL `http://dx.doi.org/10.1029/2010JD014248`. D22214.

Andrejczuk M, Reisner JM, Henson B, Dubey MK, Jeffery CA. 2008. The potential impacts of pollution on a nondrizzling stratus deck: Does aerosol number matter more than type? *Journal of Geophysical Research: Atmospheres* **113**(D19): n/a–n/a, doi:10.1029/2007JD009445, URL `http://dx.doi.org/10.1029/2007JD009445`. D19204.

Arabas S, ichiro Shima S. 2013. Large-eddy simulations of trade wind cumuli using particle-based microphysics with monte carlo coalescence. *Journal of the Atmospheric Sciences* **70**(9): 2768–2777, doi:10.1175/JAS-D-12-0295.1, URL `http://dx.doi.org/10.1175/JAS-D-12-0295.1`.

Armitage PJ. 2011. Dynamics of protoplanetary disks. *Annual Review of Astronomy and Astrophysics* **49**.

Bec J, Biferale L, Cencini M, Lanotte A, Musacchio S, Toschi F. 2007. Heavy particle concentration in turbulence at dissipative and inertial scales. *Physical review letters* **98**(8): 084 502.

Bird G. 1978. Monte carlo simulation of gas flows. *Annu. Rev. Fluid Mech.* **10**(1): 11–31.

Bird G. 1981. Monte-carlo simulation in an engineering context. *Progress in Astronautics and Aeronautics* **74**: 239–255.

Blum J, Wurm G. 2008. The growth mechanisms of macroscopic bodies in protoplanetary disks. *Ann. Rev. Astron. Astrophys.* **46**(1): 21–56, doi:10.1146/annurev.astro.46.060407.145152, URL `http://dx.doi.org/10.1146/annurev.astro.46.060407.145152`.

Bodenschatz E, Malinowski SP, Shaw RA, Stratmann F. 2010. Can we understand clouds without turbulence? *Science* **327**(5968): 970–971.

Brandenburg A. 2001. The inverse cascade and nonlinear alpha-effect in simulations of isotropic helical hydromagnetic turbulence. *Astrophys. J.* **550**(2): 824.

Brdar S, Seifert A. 2018. Mcsnow: A monte-carlo particle model for riming and aggregation of ice particles in a multidimensional microphysical phase space. *Journal of Advances in Modeling Earth Systems* **10**(1): 187–206.

Brunk BK, Koch DL, Lion LW. 1998. Turbulent coagulation of colloidal particles. *J. Fluid Mech.* **364**: 81–113.

Devenish B, Bartello P, Brenguier JL, Collins L, Grabowski W, IJzermans R, Malinowski S, Reeks M, Vassilicos J, Wang LP, *et al.* 2012. Droplet growth in warm turbulent clouds. *Quart. J. Roy. Meteorol. Soc.* **138**(667): 1401–1429.

Drakowska J, Windmark F, Dullemond CP. 2014. Modeling dust growth in protoplanetary disks: The breakthrough case. *Astron. & Astrophys.* **567**: A38, doi:10.1051/0004-6361/201423708.

Dziekan P, Pawlowska H. 2017. Stochastic coalescence in lagrangian cloud microphysics. *Atmospheric Chemistry and Physics* **17**(22): 13 509–13 520.

Falkovich G, Fouxon A, Stepanov G. 2002. Acceleration of rain initiation by cloud turbulence. *Nature* **419**: 151–154.

Grabowski WW, Wang LP. 2013. Growth of cloud droplets in a turbulent environment. *Ann. Rev. Fluid Mech.* **45**(1): 293–324, doi:10.1146/annurev-fluid-011212-140750, URL `http://dx.doi.org/10.1146/annurev-fluid-011212-140750`.

Gustavsson K, Mehlig B. 2011a. Distribution of relative velocities in turbulent aerosols. *Physical Review E* **84**(4): 045 304.

Gustavsson K, Mehlig B. 2011b. Ergodic and non-ergodic clustering of inertial particles. *Europhys. Lett.* **96**. 60012.

Gustavsson K, Mehlig B. 2014. Relative velocities of inertial particles in turbulent aerosols. *Journal of Turbulence* **15**(1): 34–69.

Gustavsson K, Mehlig B. 2016. Statistical models for spatial patterns of heavy particles in turbulence. *Advances in Physics* **65**(1): 1–57.

Gustavsson K, Mehlig B, Wilkinson M. 2015. Analysis of the correlation dimension of inertial particles. *Phys. Fluids* **27**. 073305.

Gustavsson K, Meneguz E, Reeks M, Mehlig B. 2012. Inertial-particle dynamics in turbulent flows: caustics, concentration fluctuations, and random uncorrelated motion. *New J. Phys.* **14**. 115017.

Gustavsson K, Vajedi S, Mehlig B. 2014. Clustering of particles falling in a turbulent flow. *Physical Review Letters* **112**(21): 214 501.

Johansen A, Lambrechts M. 2017. Forming planets via pebble accretion. *Annual Review of Earth and Planetary Sciences* **45**: 359–387.

Johansen A, Mac Low MM, Lacerda P, Bizzarro M. 2015. Growth of asteroids, planetary embryos, and kuiper belt objects by chondrule accretion. *Science Advances* **1**(3): e1500 109.

Johansen A, Youdin AN, Lithwick Y. 2012. Adding particle collisions to the formation of asteroids and kuiper belt objects via streaming instabilities. *Astron, Astroph.* **537**: A125.

Jorgensen WL, Chandrasekhar J, Madura JD, Impey RW, Klein ML. 1983. Comparison of simple potential functions for simulating liquid water. *J. Chem. Phys.* **79**(2): 926–935.

Kostinski AB, Shaw RA. 2005. Fluctuations and luck in droplet growth by coalescence. *Bull. Am. Met. Soc.* **86**: 235–244.

Li XY, Brandenburg A, Haugen NEL, Svensson G. 2017. Eulerian and l agrangian approaches to multidimensional condensation and collection. *J. Adv. Modeling Earth Systems* **9**(2): 1116–1137.

Li XY, Brandenburg A, Svensson G, Haugen N, Mehlig B, Rogachevskii I. 2018a. Condensational and collisional growth of cloud droplets in a turbulent environment. *arXiv preprint arXiv:1807.11859* .

Li XY, Brandenburg A, Svensson G, Haugen NE, Mehlig B, Rogachevskii I. 2018b. Effect of turbulence on collisional growth of cloud droplets. *Journal of the Atmospheric Sciences* **75**(10): 3469–3487.

Li XY, Svensson G, Brandenburg A, Haugen NE. 2018c. Cloud droplet growth due to supersaturation fluctuations in stratiform clouds. *Atmosph. Chem. Phys., submitted, arXiv:1806.10529* .

Marchioli C, Soldati A, Kuerten J, Arcen B, Taniere A, Goldensoph G, Squires K, Cargnelutti M, Portela L. 2008. Statistics of particle dispersion in direct numerical simulations of wall-bounded turbulence: Results of an international collaborative benchmark test. *Intern. J. Multiphase Flow* **34**(9): 879–893.

Miles NL, Verlinde J, Clothiaux EE. 2000. Cloud droplet size distributions in low-level stratiform clouds. *Journal of the atmospheric sciences* **57**(2): 295–311.

Naumann AK, Seifert A. 2015. A lagrangian drop model to study warm rain microphysical processes in shallow cumulus. *Journal of Advances in Modeling Earth Systems* **7**(3): 1136–1154, doi:10.1002/2015MS000456, URL `http://dx.doi.org/10.1002/2015MS000456`.

Naumann AK, Seifert A. 2016. Recirculation and growth of raindrops in simulated shallow cumulus. *Journal of Advances in Modeling Earth Systems* : n/a–n/adoi:10.1002/2016MS000631, URL `http://dx.doi.org/10.1002/2016MS000631`.

Nenes A, Seinfeld JH. 2003. Parameterization of cloud droplet formation in global climate models. *J. Geophys. Res.: Atmospheres* **108**: D14.

Ormel C, Paszun D, Dominik C, Tielens A. 2009. Dust coagulation and fragmentation in molecular clouds-i. how collisions between dust aggregates alter the dust size distribution. *Astronomy & Astrophysics* **502**(3): 845–869.

Patterson RI, Wagner W. 2012. A stochastic weighted particle method for coagulation–advection problems. *SIAM Journal on Scientific Computing* **34**(3): B290–B311.

Riechelmann T, Noh Y, Raasch S. 2012. A new method for large-eddy simulations of clouds with lagrangian droplets including the effects of turbulent collision. *New Journal of Physics* **14**(6): 065 008, URL `http://stacks.iop.org/1367-2630/14/i=6/a=065008`.

Ros K, Johansen A. 2013. Ice condensation as a planet formation mechanism. *Astronomy & Astrophysics* **552**: A137.

Saffman PG, Turner JS. 1956. On the collision of drops in turbulent clouds. *J. Fluid Mech.* **1**: 16–30, doi:10.1017/S0022112056000020, URL `http://journals.cambridge.org/article_S0022112056000020`.

Schiller L, Naumann A. 1933. Fundamental calculations in gravitational processing. *Zeitschrift Des Vereines Deutscher Ingenieure* **77**: 318–320.

Seinfeld JH, Pandis SN. 2016. *Atmospheric chemistry and physics: from air pollution to climate change*. John Wiley & Sons.

Shaw RA. 2003. Particle-turbulence interactions in atmospheric clouds. *Annu. Rev. Fluid Mech.* **35**(1): 183–227.

Shima S, Kusano K, Kawano A, Sugiyama T, Kawahara S. 2009. The super-droplet method for the numerical simulation of clouds and precipitation: a particle-based and probabilistic microphysics model coupled with a non-hydrostatic model. *Quart. J. Roy. Met. Soc.* **135**: 1307–1320, doi:10.1002/qj.441.

Siebert H, Lehmann K, Wendisch M. 2006. Observations of small-scale turbulence and energy dissipation rates in the cloudy boundary layer. *Journal of the atmospheric sciences* **63**(5): 1451–1466.

Telford JW. 1955. A new aspect of coalescence theory. *Journal of Meteorology* **12**(5): 436–444.

Unterstrasser S, Hoffmann F, Lerch M. 2017. Collection/aggregation algorithms in lagrangian cloud microphysical models: rigorous evaluation in box model simulations. *Geoscientific Model Development* **10**(4): 1521–1548, doi:10.5194/gmd-10-1521-2017, URL `https://www.geosci-model-dev.net/10/1521/2017/`.

Voßkuhle M, Pumir A, Lévêque E, Wilkinson M. 2014. Prevalence of the sling effect for enhancing collision rates in turbulent suspensions. *Journal of Fluid Mechanics* **749**: 841–852.

Wilkinson M. 2016. Large deviation analysis of rapid onset of rain showers. *Phys. Rev. Lett.* **116**: 018 501, doi:10.1103/PhysRevLett.116.018501, URL `http://link.aps.org/doi/10.1103/PhysRevLett.116.018501`.

Wilkinson M, Mehlig B, Bezuglyy V. 2006. Caustic activation of rain showers. *Phys. Rev. Lett.* **97**. 048501.

Wilkinson M, Mehlig B, Uski V. 2008. Stokes trapping and planet formation. *The Astrophysical Journal Supplement Series* **176**(2): 484.

Zsom A, Dullemond CP. 2008. A representative particle approach to coagulation and fragmentation of dust aggregates and fluid droplets. *Astron. Astrophys.* **489**(2): 931–941.

Zsom A, Ormel C, Güttler C, Blum J, Dullemond C. 2010. The outcome of protoplanetary dust growth: pebbles, boulders, or planetesimals?-ii. introducing the bouncing barrier. *Astronomy & Astrophysics* **513**: A57.